Published in final edited form as:
Nature. 2016 November 03; 539(7627): 118–122. doi:10.1038/nature19828.

Atomic model for the membrane-embedded V_o motor of a eukaryotic V-ATPase

Mohammad T. Mazhab-Jafari[1], **Alexis Rohou**[2], **Carla Schmidt**[3,†], **Stephanie A. Bueler**[1], **Samir Benlekbir**[1], **Carol V. Robinson**[3], **John L. Rubinstein**[1,4,5]

[1]Molecular Structure and Function Program, The Hospital for Sick Children, Toronto, Ontario M5G 0A4, Canada

[2]Janelia Research Campus, Howard Hughes Medical Institute, Ashburn, Virginia 20147, USA

[3]Department of Chemistry, Physical and Theoretical Chemistry Laboratory, University of Oxford, Oxford OX1 3QZ, UK

[4]Department of Medical Biophysics, University of Toronto, Toronto, Ontario M5G 1L7, Canada

[5]Department of Biochemistry, University of Toronto, Toronto, Ontario M5S 1A8, Canada

Abstract

Vacuolar-type ATPases (V-ATPases) are ATP-powered proton pumps involved in processes such as endocytosis, lysosomal degradation, secondary transport, TOR signalling, and osteoclast and kidney function. ATP hydrolysis in the soluble catalytic V_1 region drives proton translocation through the membrane-embedded V_O region via rotation of a rotor subcomplex. Variability in the structure of the intact enzyme has prevented construction of an atomic model for the membrane-embedded motor of any rotary ATPase[1–5]. We induced dissociation and auto-inhibition of the V_1 and V_O regions of the V-ATPase by starving the yeast *Saccharomyces cerevisiae*[6,7], allowing us to obtain a ~3.9-Å resolution electron cryomicroscopy map of the V_O complex and build atomic models for the majority of its subunits. The analysis reveals the structures of subunits $ac_8c'c''de$ and a protein that we identify and propose to be a new subunit (subunit f). A large cavity between subunit a and the c-ring creates a cytoplasmic half-channel for protons. The c-ring has an asymmetric distribution of proton-carrying Glu residues, with the Glu residue of subunit c″ interacting with Arg735 of subunit a. The structure suggests sequential protonation and

Correspondence and requests for materials should be addressed to J.L.R. (john.rubinstein@utoronto.ca).
†Present address: Interdisciplinary Research Center HALOmem, Martin Luther University, Halle-Wittenberg, 06120 Halle (Saale), Germany.

Author Contributions M.T.M.-J. prepared yeast strains, purified protein, prepared cryo-EM specimens, performed 200 kV cryo-EM and Relion image analysis, and built the atomic models. A.R. collected and pre-processed data with the 300-kV microscope and performed image analysis with Frealign. C.S. performed the mass spectrometry analysis. S.A.B. prepared yeast strains and assisted with protein purification. S.B. assisted with cryo-EM specimen preparation and screening. C.V.R. supervised mass spectrometry experiments, and J.L.R. supervised the other aspects of the work and coordinated experiments. J.L.R. and M.T.M.-J. wrote the manuscript and prepared the figures with input from the other authors.

Author Information Cryo-EM maps have been deposited in the Electron Microscopy Data Bank under accession numbers EMD-8363, EMD-8364, EMD-8367, and EMD-8409. The atomic model has been deposited in the Protein Data Bank under accession number 5TJ5. Reprints and permissions information is available at www.nature.com/reprints. The authors declare no competing financial interests. Readers are welcome to comment on the online version of the paper.

Reviewer Information Nature thanks A. Hack, K. Parra, H. Saibil and J. Weber for their contribution to the peer review of this work.

Europe PMC Funders Author Manuscripts

deprotonation of the c-ring, with ATP-hydrolysis-driven rotation causing protonation of a Glu residue at the cytoplasmic half-channel and subsequent deprotonation of a Glu residue at a luminal half-channel.

Following starvation-induced dissociation of the V_1 and V_O regions of V-ATPase, the auto-inhibited V_O complex is markedly more structurally homogeneous than in the intact V-ATPase[1]. Our 3D electron cryomicroscopy (cryo-EM) map reveals the structure of the intact V_O complex (Fig. 1a–c, Extended Data Fig. 1 and Supplementary Table 1) with an overall resolution of 3.9 Å (Extended Data Fig. 2). Although the resolution is variable throughout the map (Extended Data Fig. 2c), side-chain densities are apparent for most of the α-helices in the complex, allowing for the construction of an atomic model (Fig. 1d and Extended Data Fig. 3). A few regions (for example, subunits $c_{(5)}$ and $c_{(6)}$ in Extended Data Fig. 3g) only have sufficient resolution to model large side chains; however this still allows the protein sequence to be placed in register in the map. Resolution was poorest for the soluble domain of subunit a where it contacts subunit d, which we modelled entirely as poly-alanine. The map reveals the structures of the $c_8c'c''$-ring (Fig. 1a, pink, magenta and purple), subunit a (Fig. 1a, green), subunit d (Fig. 1a, cyan), and two additional proteins. These additional components were detected in a lower-resolution analysis of the intact V-ATPase complex[1,5], but can be seen here to consist of two transmembrane α-helices each (Fig. 1b, c, blue and red–brown). Both of these proteins appear to be stoichiometric components of the complex, as suggested by their relative densities in the map. One of these subunits (Fig. 1b, c, red–brown) abuts α-helix 2 and the loop connecting α-helices 7 and 8 of subunit a. The other protein is an α-helical hairpin that contacts α-helix 1 of subunit a (Fig. 1b, c, blue). These two proteins are discussed in more detail later on.

Subunit d sits on top of the c-ring, linking the V_1 and V_O parts of the central rotor. As seen previously in an ~18-Å resolution map of the V_O complex[8], subunit d sits deeper within the c-ring in the V_O complex than it does in the intact V-ATPase[1]. In contrast to the intact V-ATPase structure, in the V_O complex the N-terminal domain of subunit a from the stator part of the enzyme is in contact with subunit d from the rotor[1,8,9]. This interaction would prevent rotation of the c-ring, consistent with the observation that the V_O complex is impermeable to protons when separated from the V_1 region[6,7]. However, the V_O complex remains impermeable to protons even when subunit d or the N-terminal domain of subunit a are removed[8,10]. Furthermore, we also identified a 3D class that lacks subunit d but otherwise appears to have almost the same structure as the intact V_O complex (Extended Data Fig. 4). Consequently, the movement of the N-terminal domain of subunit a, and inhibition of proton translocation, cannot be due to interaction of the N-terminal domain of subunit a with subunit d.

The fold of subunit a is consistent with the fold predicted by lower-resolution cryo-EM studies of the intact V-ATPase combined with evolutionary covariance analysis[5]. The subunit contains eight membrane-embedded α-helices, with structured loops connecting some of these α-helices. The membrane-embedded domain of subunit a starts with a pair of short α-helices that do not fully cross the lipid bilayer (Fig. 1b, c, α-helices a_1 and a_2). Four subsequent transmembrane α-helices (a_3 to a_6) produce a central layer in the subunit

structure, which terminates with two long and highly-tilted transmembrane α-helices that contact the c-ring (a_7 and a_8) and are characteristic of rotary ATPases[1–3,5]. No density was detected for the loop between residues 659 and 709, which is the region with the least sequence similarity amongst the different isoforms of subunit a[5]. The lack of density for this loop suggests that it is mobile in the structure. Another loop (residues 481–523) could also not be modelled, although a region of low-resolution density in the map (Fig. 1b, semi-transparent grey density) probably corresponds to this loop and to parts of the two small membrane-embedded proteins in the V_O complex.

Unlike the c-ring of F-type ATP synthases and bacterial V/A-ATPases, the proton-carrying ring of the eukaryotic V-ATPase is hetero-oligomeric. The *S. cerevisiae* V-ATPase $c_8c'c''$-ring has 40 transmembrane α-helices arranged into an inner ring and outer ring of 20 α-helices each[1,11] (Fig. 2). Each c, c′, and c″ subunit contributes four α-helices to the c-ring, two to the inner ring and two to the outer ring. The cryo-EM map shows two additional α-helices that pass through the $c_8c'c''$-ring (Fig. 2b, purple asterisk). These α-helices can be attributed to 56 residues at the N terminus of subunit c″ (ref. 12), most of which are not necessary for proton translocation[13] and correspond to density previously seen within the c-ring[14] and upon re-examination of the intact V-ATPase maps[1]. The first additional α-helix is adjacent to subunit $c_{(1)}$ and the second is near the centre of the c-ring with a clear connection to the rest of subunit c″. Although map resolution is limited in this region, it is sufficient to register the sequence of the α-helices (Extended Data Fig. 3b). This structure for subunit c″ differs from a crystal structure of a bacterial hybrid 'F/V'-ATPase c-ring, in which a single additional N-terminal helix lay across the periplasmic surface of the ring[15]. Subunit c″ serves as the main contact between subunit d and the c-ring (Fig. 1a, bottom, cyan asterisk), making it critical for the transmission of ATP-driven rotation of subunits D and F of the V_1 region to the c-ring of the V_O region. Comparison to the lower-resolution cryo-EM maps of the intact V-ATPase[1] (Extended Data Fig. 5a–c) shows that the V_O complex is in the least populated, and probably the least stable, of the three rotational states identified for the intact enzyme (Extended Data Fig. 5d). Therefore, subunit c″ apparently marks the position of the c-ring from which the complex can disassemble and reassemble[6,7]. An unexpected feature of the subunit c″ structure is the location of its essential proton-carrying Glu residue[12]. Each c, c′, and c″ subunit has a single proton-carrying Glu residue (Glu137, 145, and 108, respectively[12]), giving 10 proton-carrying residues for the 20 outer α-helices of the ring. Notably, the Glu residue of subunit c″ is on its second ring-forming α-helix, whereas in subunits c and c′ it is found on the fourth ring-forming α-helix. This arrangement gives an irregular distribution of acidic proton-carrying Glu residues, rather than having proton-binding sites on alternating α-helices (Fig. 2b, right, in red). The two adjacent negative charges of subunits c″ and $c_{(1)}$ that are in contact with subunit a may determine the disassembly- and reassembly-competent conformations of the enzyme.

Transmembrane proton pumping is thought to occur via two offset half-channels: a cytoplasmic half-channel that protonates Glu residues of the c-ring and a luminal half-channel that deprotonates Glu residues[16,17]. The cytoplasmic half-channel, which leads to Glu108 of subunit c″, is readily apparent from inspection of the model as a deep cavity between the c-ring and the two highly tilted α-helices of subunit a (Fig. 3a, b, blue density and arrow). At its opening to the cytoplasm, this cavity is almost 20 Å across and 10 Å wide

and is predicted to be filled with water[18], providing direct access to Glu108 for protons from the cytoplasm. The location of this channel, at the interface of subunit a and the c-ring, is consistent with biochemical experiments[19,20] and with the indentations observed in the detergent micelles of lower-resolution cryo-EM density maps of the F-, V/A-, and V-type ATPases[1–3,5]. The position of the cytoplasmic half-channel places it in close proximity to the loop of 51 residues between α-helices a_5 and a_6 (659–709), which contains 21 charged residues[5]. This loop may be involved in modulating access to the half-channel[5]. The location of the luminal half-channel is less obvious. Inspection of lower-resolution cryo-EM maps suggested the presence of a gap in the detergent micelle[21]. Consideration of residues conserved across species suggested a proton path that involves the first and second membrane-embedded α-helices of subunit a[5] (Fig. 1c, a_2 and a_3). If this position is the presumed location of the luminal half-channel, its exit is thus located near to the region of unmodelled density in the cryo-EM map (Fig. 3a, grey mesh). However, a clear path through the protein, from the centre of the lipid bilayer to its luminal surface, is not readily apparent from the model and could not be detected through automated identification of potential pore-lining residues[22] or by searching for gaps in the protein[23]. It should be recalled that the dissociated V_O region is auto-inhibited and does not allow for proton translocation[6,8] and therefore the luminal half-channel may not exist in this state. Alternatively, the luminal half-channel may remain closed in proton-pumping V-ATPases, only opening transiently during proton translocation. Future investigation of the path that protons take from the centre of the lipid bilayer to the lumen is therefore warranted.

All rotary ATPase a subunits include an essential Arg residue (Arg735 in the *S. cerevisiae* V-ATPase) that is necessary to couple ATP synthesis or hydrolysis to proton translocation[24,25]. The conserved Glu residues of subunits c, c′, and c″ are also essential for proton transport in the V-ATPase[12]. In the auto-inhibited V_O complex, Glu108 of subunit c″ interacts with Arg735 present on the penultimate α-helix of subunit a[5] (Fig. 3c). This interaction suggests that Glu108 is deprotonated. The presumed salt bridge between Arg735 and Glu108 is similar to those between Arg–Asp pairs shown to ensure proton selectivity in voltage-gated proton channels[26]. However, because rotary ATPases can transport different ions and the architecture of rotary ATPases appears to be generally conserved, the function of the Arg–Glu pair here is probably to ensure that the Glu residue is stripped of its ion before it leaves the luminal half-channel, rather than to ensure proton specificity.

Liquid chromatography–tandem mass spectrometry (LC–MS/MS) analysis of in-gel-digested protein suggested that Vma9p (subunit e) and putative protein YPR170W-B were present in the purified V_O complex (Supplementary Table 2 and Supplementary Data). The α-helical hairpin shown in blue in Fig. 1a–c was identified as subunit e because its density fit with that of the three Trp residues and the Phe and Tyr residues of subunit e (Extended Data Fig. 3e). The structure of subunit e, and the interaction of its C terminus with a loop in subunit a, explains why addition of a C-terminal affinity tag to subunit e causes its dissociation from the detergent-solubilized complex[27]. Its position distal to the area of interaction between subunit a and the c-ring is consistent with the observation that its removal from the assembled V-ATPase does not affect proton-pumping activity[27]. Deletion of the *VMA9* gene leads to the conditionally lethal VMA phenotype[28] and the absence of V-ATPase from the yeast vacuole, suggesting that subunit e is necessary for the successful

localization and assembly of the complex[29]. To confirm the presence of putative protein YPR170W-B as the additional membrane-embedded component of the V_O complex, we constructed a *S. cerevisae* strain with a 3×FLAG-tag fused to the C terminus of YPR170W-B. Affinity purification from the detergent-solubilized membranes of this strain isolated the V_O complex with some subunits from the intact V-ATPase (Extended Data Fig. 6a), confirming the protein as a component of the V_O complex. We subsequently purified the V_O complex from a strain of yeast lacking YPR170W-B and determined its structure by cryo-EM (Extended Data Fig. 6b). The missing density in the 3D map allowed us to unambiguously locate YPR170W-B in the complex. Deletion of YPR170W-B, which we now tentatively identify as subunit f of the V-ATPase, did not produce the VMA phenotype[28] (Extended Data Fig. 6c), indicating that it is not essential for V-ATPase localization or for proton pumping. The peripheral location of the protein, away from the interface of subunit a and the c-ring, leaves its function in the V-ATPase complex unclear. A BLAST search indicates that YPR170W-B is highly conserved in fungi. Reliable identification of possible animal or plant homologues of subunit f will require experiments with other organisms. The cryo-EM density for YPR170W-B (red–brown in Fig. 1) had insufficient resolution to build an atomic model; consequently this component of the complex was modelled as poly-alanine.

The asymmetric distribution of Glu residues around the c-ring, and how the ring interacts with subunit a, has implications for possible modes of proton translocation. The spacing between Glu residues in the c-ring has an increment of 36° between most Glu residues, but 18° between the Glu residues of subunits c'' and $c_{(1)}$ (Fig. 2b, purple and light pink), and 54° between the Glu residues of subunits c' and c'' (Fig. 2b, magenta and purple). As seen in this model, subunit c'' is positioned at the protonating cytoplasmic half-channel (Fig. 4a, blue arrow). In this orientation, subunit $c_{(1)}$ is in contact with subunit a at a possible mid-membrane origin for the luminal half-channel (Fig. 4a, red arrow). However, if the ring were rotated such that one of the c subunits (for example, subunit $c_{(1)}$) engages with the cytoplasmic half-channel (Fig. 4b, blue arrow) then the next c subunit (subunit $c_{(2)}$ in this example) would not be in contact with subunit a, making it unlikely that it is near a luminal half-channel (Fig. 4b, red arrow). Misalignment with any possible luminal half-channel is even more pronounced if subunit c' is engaged with the cytoplasmic half-channel (Fig. 4c, blue arrow), in which case the Glu from subunit c'' is extremely far from contact with subunit a (Fig. 4c, red arrow). This mismatch ensures that protonation and deprotonation cannot always occur simultaneously. Instead, the sequence of events for ATP-hydrolysis-driven proton pumping must be that rotation of the c-ring, caused by ATP hydrolysis in the V_1 region, breaks the contact between Arg735 and a deprotonated Glu residue, dragging the Glu residue into the hydrophobic environment of the lipid bilayer (Fig. 4d). Thermodynamic analysis has shown that moving a deprotonated Glu residue from an aqueous environment into the middle of a hydrophobic lipid bilayer will force the residue to acquire a proton and become neutralized[30]. This thermodynamic property of Glu residues ensures that the ring does not ‘slip’, allowing a deprotonated Glu to move into the lipid bilayer, which would uncouple ATP hydrolysis from proton pumping. Rotation of the c-ring brings a protonated Glu residue out of the lipid bilayer and into alignment with the putative luminal half-channel. As rotation of the ring continues, the Glu residue encounters Arg735, possibly in a

different orientation than observed in this structure, causing deprotonation of the Glu residue via the luminal half-channel and resetting the c-ring for a subsequent protonation–deprotonation cycle. The conformation of Arg735 may also need to adapt to accommodate interaction with the Glu residue of subunit c″, compared to subunit c or c′. This sequence of events, in which only one Glu residue at a time interacts with a half-channel, explains how rotary ATPases can tolerate c-rings with variable21 and unequal distances between the c-subunits.

Methods

Yeast strains and protein purification

To isolate the *S. cerevisiae* V_O complex, yeast strain CACY1, expressing Vph1p (subunit a) with a 3×FLAG-tag at its C terminus, was prepared by homologous recombination as described previously[9]. To confirm that YPR170W-B is a subunit of the V-ATPase, an *S. cerevisiae* strain was prepared with a 3×FLAG-tag fused to the C terminus of the uncharacterized open reading frame *YPR170W-B (Saccharomyces* genome database identifier S000028515) in the protease-deficient background strain MM93, producing the strain SABY87. To purify intact V-ATPase, we used strain SABY31, which bears a 3×FLAG-tag on Vma1p and with the *STV1* gene deleted[9]. *YPR170W-B* was deleted in strain CACY1 by homologous recombination with the NatR cassette to produce strain MMJY1 as previously described[9]. Western blotting against 3×FLAG-tagged proteins was done with the monoclonal anti-FLAG antibody M2 (Sigma). For protein purification, yeast in YPD medium were grown in an 11-l BioFlo fermenter (New Brunswick Scientific) for 60 h in order to induce nutrient starvation and dissociation of the V_1 and V_O regions of the complex. V_O complex solubilized with dodecylmaltoside (DDM) was purified via the 3×FLAG-tag with M2 affinity matrix (Sigma), following the same protocol used for the intact V-ATPase[3,9]. After purification in elution buffer (50 mM Tris-HCl pH 7.5, 150 mM NaCl, 0.02% (w/v) DDM, 50 μg/ml 3×FLAG peptide), the V_O complex was mixed with amphipol A8-35 (Anatrace) at a protein:amphipol ratio of 1:10 (w/w) with gentle agitation for 1 h. Detergent was removed with 15 mg/ml Bio-Beads SM-2 (Bio-rad) at 4 °C overnight. The sample was purified further with a Superdex 200 column previously equilibrated with buffer (50 mM Tris-HCl pH 7.5, 150 mM NaCl). Protein from the chromatographic peak corresponding to the V_O complex was collected and concentrated to 2.5 mg/ml with a 100-kDa MWCO Amicon concentrator (Millipore) and bafilomycin A1 was added to 10 μM (Santa Cruz Biotechnology) before further analysis.

LC–MS/MS and database search

Subunits of the V_O preparation were separated by SDS–PAGE and regions of the gel were excised at positions where small trans-membrane α-helical hairpin subunits are expected. Proteins were digested in the gel as described previously[31] with trypsin and chymotrypsin at 37 °C and 25 °C, respectively. For combined tryptic and chymotryptic digestion, proteins were digested with trypsin at 37 °C for 3 h before chymotrypsin was added and the sample was incubated at 25 °C overnight. Peptides dissolved in 2% (v/v) acetonitrile and 0.1% (v/v) formic acid were separated by nano-flow liquid chromatography (Dionex UltiMate 3000 RSLC, Thermo scientific; mobile phase A: 0.1% (v/v) formic acid; mobile phase B: 80%

Europe PMC Funders Author Manuscripts

(v/v) acetonitrile, 0.08% (v/v) formic acid). Peptides were then loaded onto a trap column (Reprosil C18, 100 μm inner diameter, particle size 5 μm; Dr. Maisch GmbH, prepared in-house) and separated with a flow rate of 300 nl/min on an analytical C18 capillary column (Reprosil C18, 75 μm inner diameter, particle size 1.9 μm, 27–28 cm; Dr. Maisch GmbH, prepared in-house), with a gradient of 5–90% (v/v) mobile phase B over 46 min. Separated peptides were directly eluted into a Orbitrap Fusion Tribrid Mass Spectrometer (Thermo scientific). Typical mass spectrometric conditions were: spray voltage of 2.3 kV; capillary temperature of 275 °C; collision energy of 30%, activation Q of 0.25. The Orbitrap Fusion Tribrid Mass Spectrometer was operated in data-dependent mode. Survey full-scan MS spectra were acquired in the orbitrap (m/z 380−1,500) with a resolution of 120,000 and an automatic gain control (AGC) target at 400,000. The top-10 most intense ions were selected for higher-energy collisional dissociation MS/MS fragmentation in the orbitrap at a resolution of 30,000 and an AGC target of 1,200 and with a first m/z of 110. Dynamic exclusion of previously selected ions was set to 30 s. Only ions with charge states 2–7 were selected. Singly and doubly charged ions, as well as ions with an unrecognized charge state, were also excluded. Internal calibration of the orbitrap was performed with the lock mass option (lock mass, m/z 445.120025)[32]. Raw files were converted into mgf files using Proteome Discoverer (Thermo scientific). Mgf files were searched against Uniprot_Yeast database (23,481 sequences) using Mascot search engine v2.03.2002 (Matrix Science). Search parameters were: peptide mass tolerance, 10 p.p.m.; fragment mass tolerance, 0.6 Da; enzyme, trypsin; variable modifications, carbamidomethylation (cysteine) and oxidation (methionine).

Cryo-EM and image analysis

V_O complex (2.5 μl) in amphipol was applied to nano-fabricated, holey-gold-coated EM grids[33] previously glow-discharged in air for 15 s, blotted for 15 s, and then plunge-frozen with a modified Vitrobot grid-preparation device (FEI Company) in a mixture of liquid ethane and propane at liquid-nitrogen temperature[34]. Cryo-EM grid preparation conditions were optimized and a small dataset consisting of 1,082 images obtained with a field-emission Tecnai F20 electron microscope (FEI Company) operating at 200 kV, with images recorded on a Gatan K2 Summit (Gatan Inc.) direct detector device camera (counting mode, 2 frames/s, 15 s, 1.45 Å/pixel, 1.2 e^{-}/Å^2/frame). An initial model for the V_O complex was generated by manually segmenting a map of the intact V-ATPase[1] with UCSF Chimera[35] and low-pass filtering to 30 Å. Image analysis with Alignframes_lmbfgs[36], CTFFIND3 (ref. 37). Alignparts_lmbfgs[36], magnification anisotropy correction[38] and Relion 1.3 (ref. 39) produced a preliminary map at 6.8-Å resolution from 39,384 particle images. The structure of the V_O complex in DDM was also determined from yeast strains CACY1 (wild type) and MMJY1 (ΔYPR170W-B). These specimens were prepared with nanofabricated holeycarbon-coated EM grids subjected to glow-discharge for 2 min and blotted for 20 s. 3D maps were calculated at 8.3-Å resolution from 43,184 particle images (for CACY1) and at 8.7-Å resolution from 44,468 particle images (for MMJY1).

For high-resolution image acquisition, grids were sent in a cryogenic specimen shipper to the HHMI Janelia Research Campus where they were imaged with a Titan Krios electron microscope (FEI Company). Micrographs were recorded from a single grid with the

microscope operated at 300 kV using parallel illumination at 4.8 $e^{-}/Å^2/s$ of a 1.58-μm diameter region of the grid from a 70-μm objective aperture. Images were recorded with a K2 Summit direct detector device camera operating in super-resolution mode with a nominal magnification of 37,000×. With no specimen present in the optical path, the rate of exposure of the detector was 3 e^{-}/pixel/s. Dose-fractionated exposures of 21 s were recorded as movies with 70 frames, so that selected specimen areas were exposed to a total of 100 $e^{-}/Å^2$. Data collection was automated with SerialEM[40]. A previously measured magnification anisotropy was corrected with the program mag_distortion_correct[41], leading to a super-resolution pixel size of 0.3885 Å. Frames were down-sampled to a pixel size of 1.554 Å by Fourier-space cropping and aligned with each other using Unblur[42]. Probably because of the high magnification and small field of view, no apparent advantage was detected for correcting images for individual particle motion[36]. Defocus parameters were estimated with CTFFIND4 (ref. 43) from the average of amplitude spectra of sums of 3 unaligned frames resampled to a pixel size of 1.94 Å. 657,975 particle images were automatically selected with Relion from 4,365 aligned and averaged movies, and extracted into 200 × 200 pixel boxes. 2D classification with Relion reduced the dataset to 462,842 particle images.

The map showing the V_O complex lacking subunit d was obtained by 3D classification and refinement with Relion (ref. [39]). The 6.8-Å resolution map of the V_O complex in amphipol from the Tecnai F20 dataset was used as a starting reference for aligning the full dataset of particle images with Frealign[44]. In all subsequent processing steps, information beyond 6-Å resolution was excluded to prevent over-fitting of noise at higher resolutions. Initial particle orientation parameters were obtained by 1 cycle of grid search in Frealign mode 3, using an angular step size of 3.4°. Following this cycle, and before every subsequent cycle, the solvent and amphipol regions of the map were low-pass-filtered to 30 Å to reduce the fitting of noise from solvent and amphipol densities[45]. Final particle-orientation parameters were obtained after 19 cycles of local refinement (mode 1), one cycle of mode 3 exhaustive search, and 11 further cycles of local refinement. The final 3D map was calculated from particle images padded with zeroes from 200 × 200 to 400 × 400 pixels to mitigate CTF aliasing effects[46] and was then cropped to a 200 × 200 × 200 voxel volume. Overall resolution of the map was estimated by Fourier shell correlation to be 3.9 Å. Local resolution variability was estimated with blocres[47].

Model building

Most regions of the map, particularly membrane-embedded α-helices, had sufficient details to allow *de novo* model building. Initial models for subunits c, c′, c″, d, and the N-terminal domain of subunit a were generated with the SWISS-MODEL server[48] using a model of intact V-ATPase from cryo-EM (Protein Databank accession number 3J9V) as a template. The initial model for the membrane-embedded domain of subunit a was from the cryo-EM and evolutionary covariance analysis of that protein (Protein Databank accession number 5I1M)[5]. Initial models for subunits e and f were generated manually in Coot[49]. Initial models were fit into density as rigid bodies with UCSF Chimera[35]. Final models were built with successive rounds of real-space refinement in Phenix[50] and manual model building in Coot and gave an EMRinger score of 2.0 for the entire model[51], which is superior to the typical score of 1.0 for a 4-Å map. 93.2, 6.3, and 0.5% of residues were in preferred,

allowed, and disallowed regions of the Ramachandran plot, respectively, with no Ramachandran outliers in the α-helical regions of the model. Where no corresponding densities were observed, side chains were deleted while maintaining the residue identity. Subunit f and the N-terminal domain of subunit a were modelled entirely as poly-alanine.

Extended Data

Europe PMC Funders Author Manuscripts

Europe PMC Funders Author Manuscripts

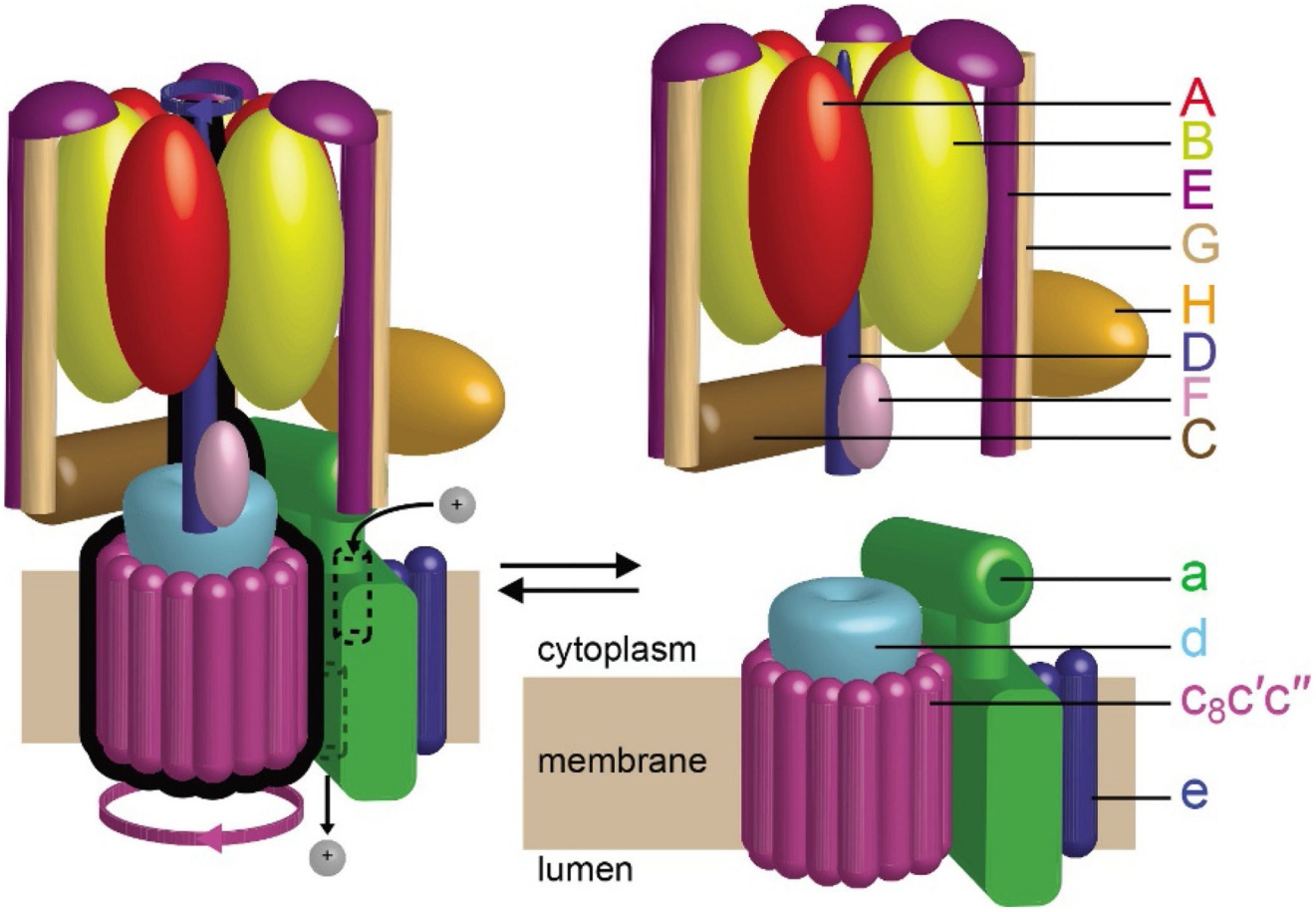

Extended Data Figure 1. Subunit composition of the intact V-ATPase and dissociated V_1 and V_O regions.

The rotor is outlined in black and the two half-channels in the V_O region are indicated with dashed lines. The intact V-ATPase (left) dissociates into the auto-inhibited V_1 and V_O complexes upon nutrient starvation. Figure adapted from ref. 1.

Europe PMC Funders Author Manuscripts

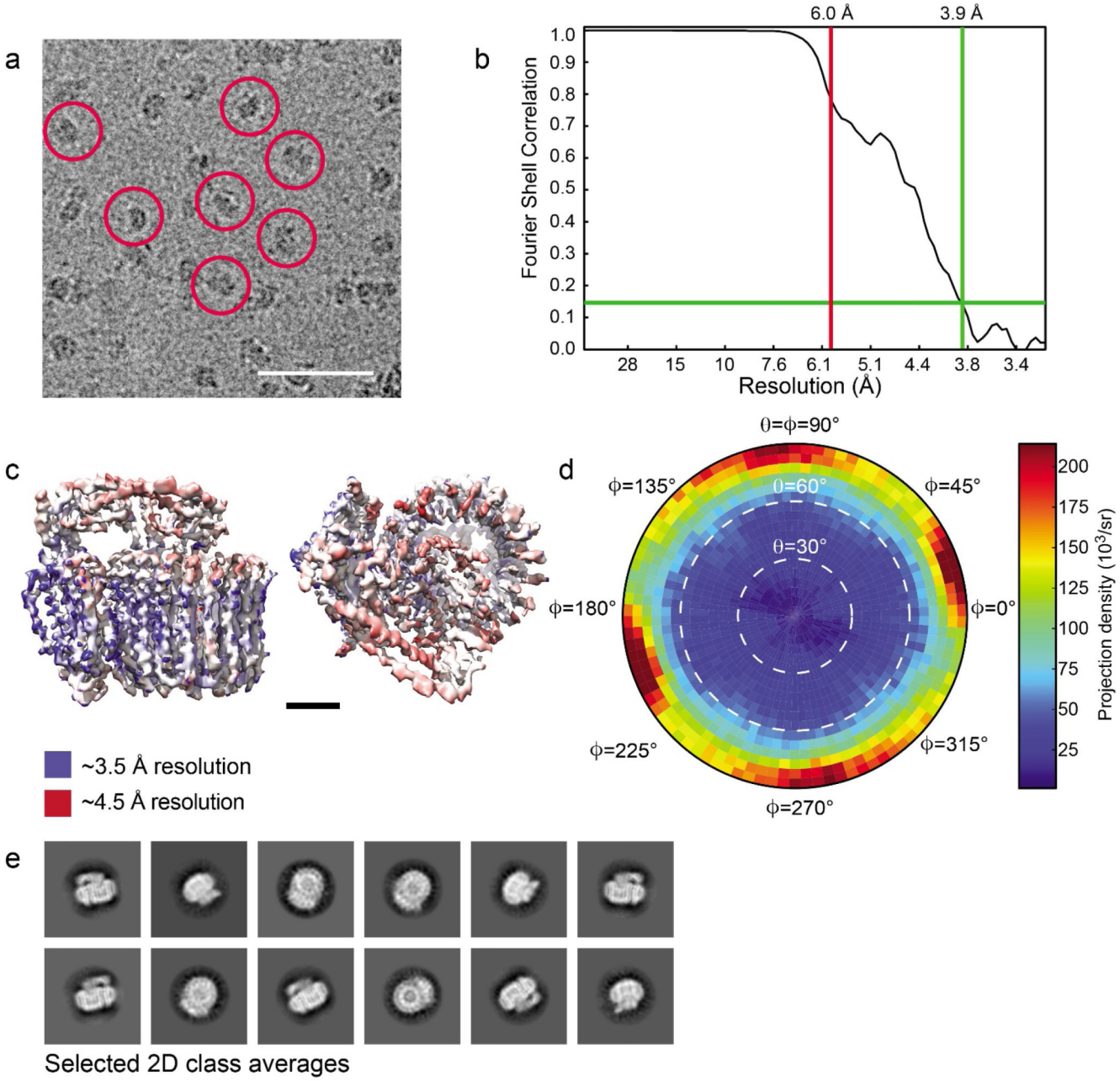

Extended Data Figure 2. Cryo-EM map generation.

a, An example micrograph with protein particles circled in red. Scale bar, 500 Å. **b**, Fourier shell correlation (FSC) curve. The highest-resolution information used in image alignment (6 Å) and the overall resolution of the map at FSC = 0.143 (3.9 Å) are indicated. **c**, Local resolution assessment. Scale bar, 25 Å. **d**, Image orientation distribution. **e**, Example 2D class average images.

Europe PMC Funders Author Manuscripts

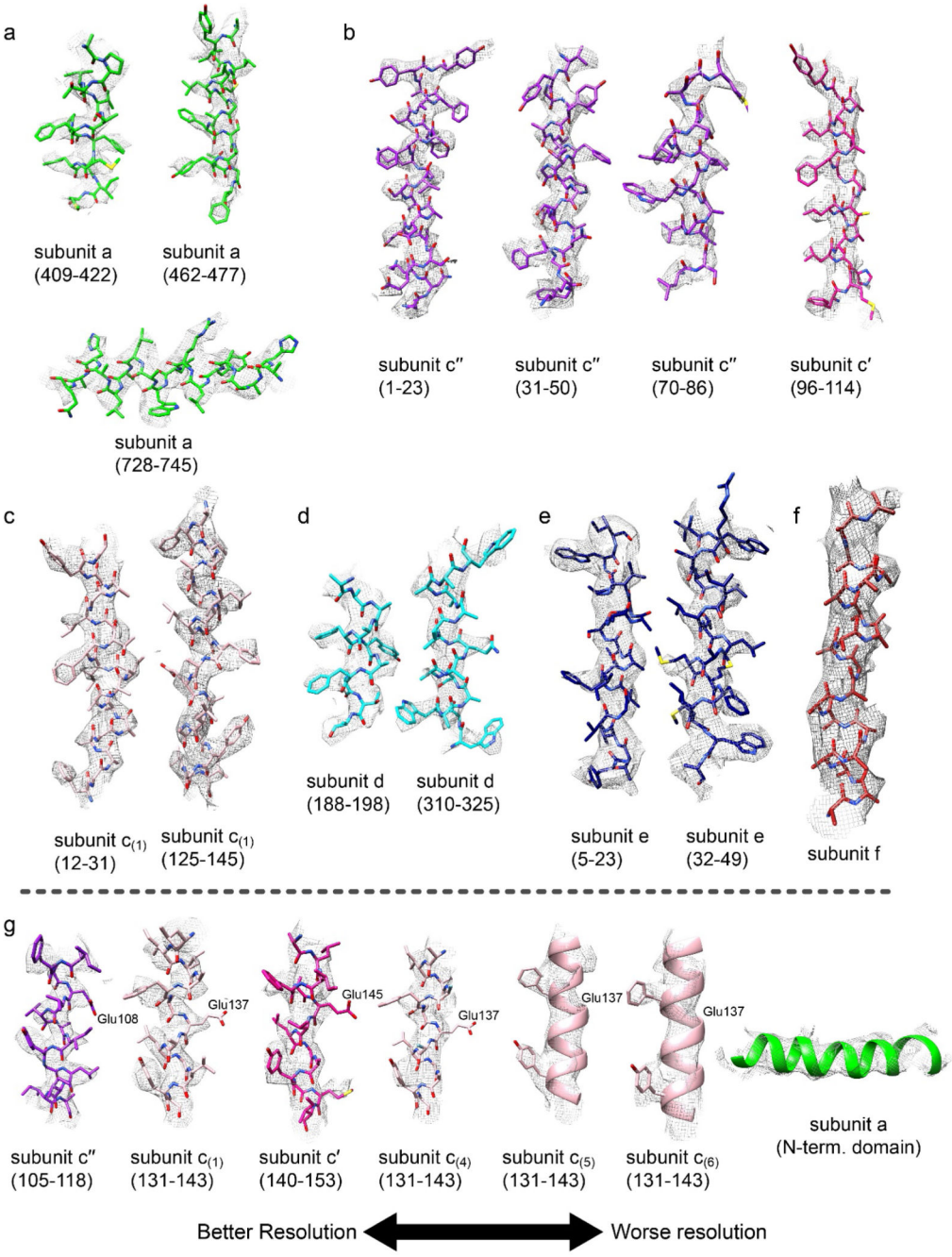

Extended Data Figure 3. Model building.

a–**f**, Example regions of the atomic model built for subunits a (**a**), c″ and c′ (**b**), $c_{(1)}$ (**c**), d (**d**), e (**e**), and f (**f**). **g**, The different α-helices from the c-ring bearing conserved Glu residues show variable resolution. An α-helix from the N-terminal domain of subunit a has poor resolution. Residue numbers are shown in brackets.

Europe PMC Funders Author Manuscripts

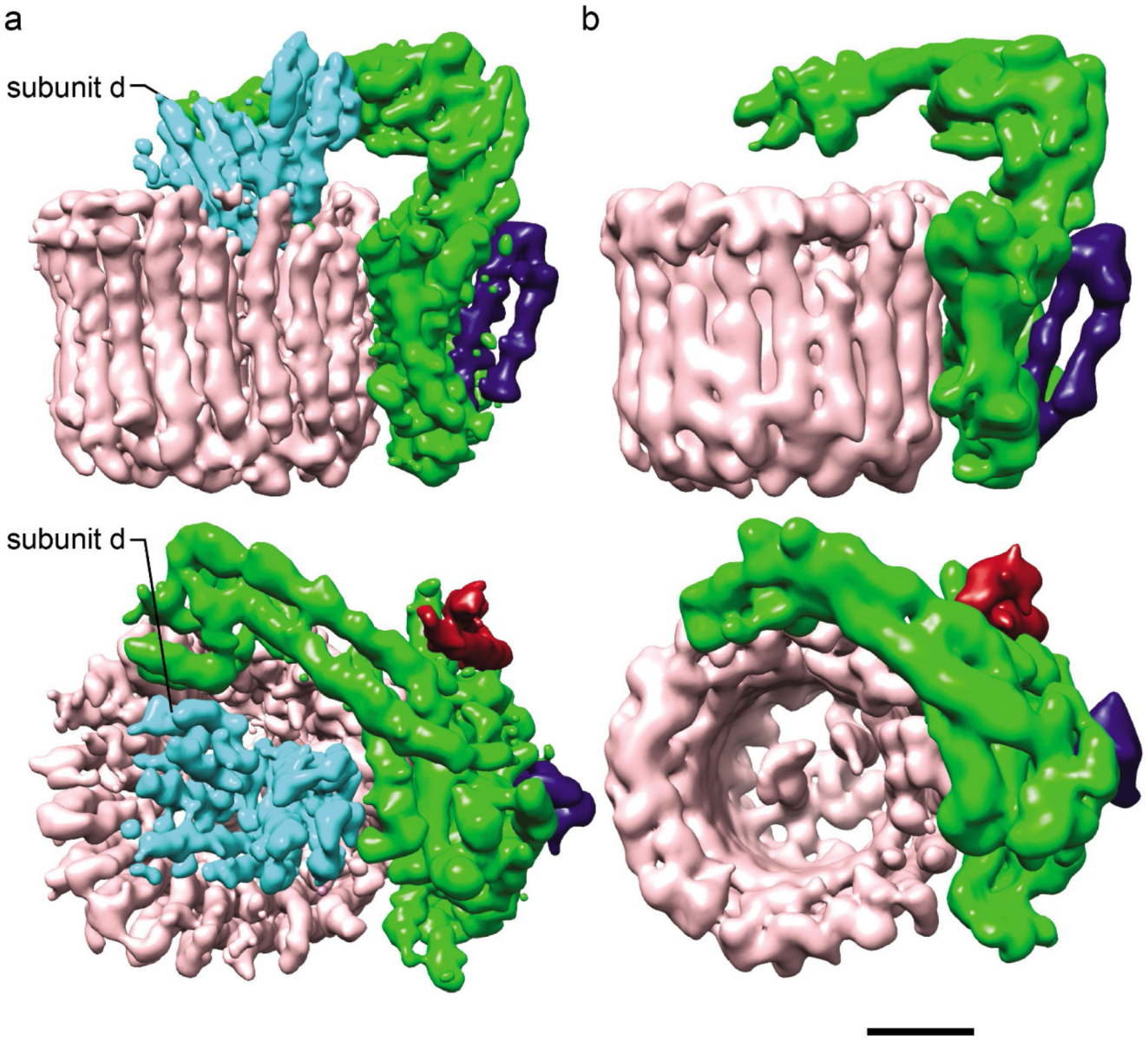

Extended Data Figure 4. V_O complex lacking subunit d.

a, The V_O complex map from all of the particle images shows subunit d. **b**, V_O complex map from a 3D class, containing 24,744 particle images, that lacks subunit d was determined at 7.8-Å resolution. Scale bar, 25 Å.

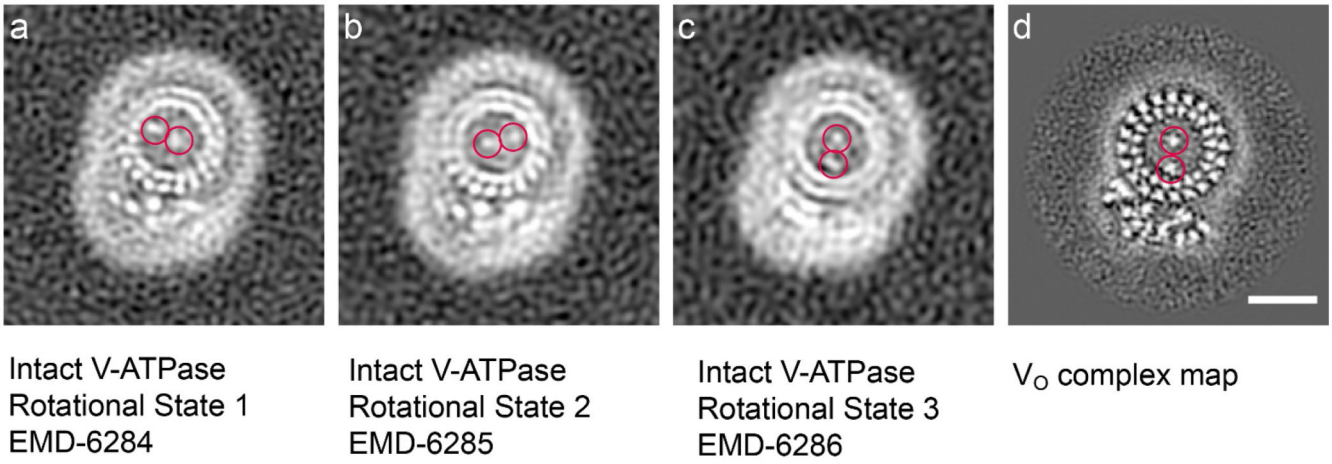

Extended Data Figure 5. V_O complex is in rotational state 3.

a–**c**, rotational states 1, 2, and 3 of the intact V-ATPase show the two α helices of subunit c" within the c-ring[1]. **d**, The two α-helices of subunit c″ within the c-ring show the ring to be in the same orientation as in rotational state 3 of the intact V-ATPase. Scale bar, 25 Å.

Europe PMC Funders Author Manuscripts

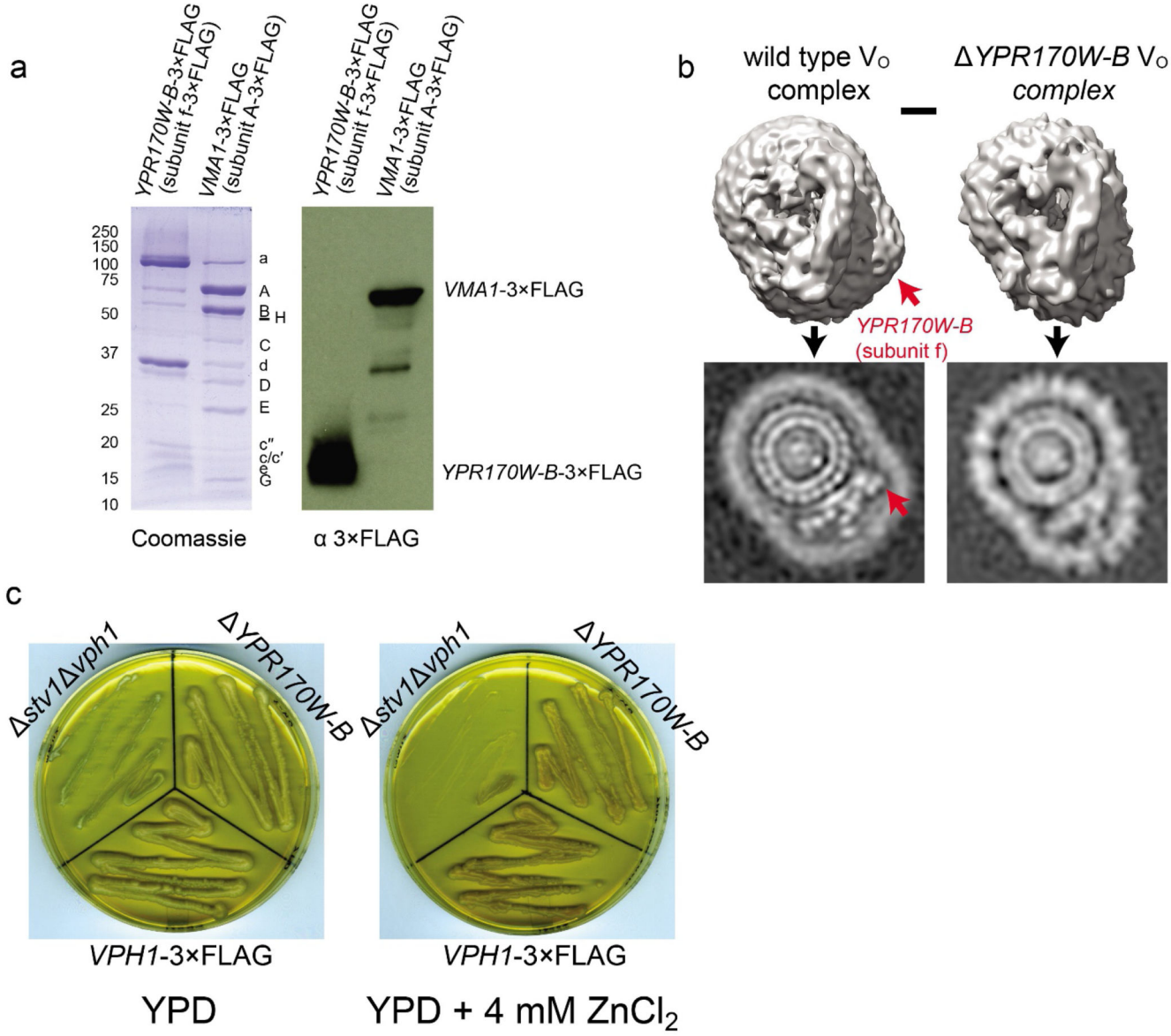

Extended Data Figure 6. Identification of subunit f.

a, SDS–PAGE gel (left) and western blot (right) against a 3×FLAG-tag for the affinity purification of 3×FLAG-tagged YPR170W-B (subunit f) and Vma1p (subunit A) show that both proteins are components of the V-ATPase. **b**, Surface-rendered 3D maps (upper) and map cross-sections (lower) showing the wild-type V_O complex (left) and the V_O complex from a yeast strain with the *YPR170W-B* gene deleted (right). Density from YPR170W-B is indicated with a red arrow. Scale bar, 25 Å. **c**, Yeast strains with the *STV1* and *VPH1* genes deleted, the *STV1* and *YPR170W-B* gene deleted, and only *STV1* gene deleted were grown on both YPD medium (left) and YPD medium with zinc (right), demonstrating that deletion of *YPR170W-B* does not cause the VMA phenotype.

Supplementary Material

Refer to Web version on PubMed Central for supplementary material.

Acknowledgements

We thank N. Grigorieff for providing access to the Titan Krios electron microscope and H. Urlaub for providing C.S. with access to mass spectrometry instrumentation while in Göttingen. We thank Z. Ripstein, P. Tieleman, R. Pomès, and J.-P. Julien for discussions and J. Zhao, J.-P. Julien and V. Kanelis for a critical reading of the manuscript. M.T.M.-J. was supported by a Postdoctoral Fellowship from the Canadian Institutes of Health Research (CIHR), C.V.R. is a Royal Society Professor and J.L.R. holds a Canada Research Chair. This work was supported by operating grant MOP81294 from the Canadian Institutes of Health Research (J.L.R.), Wellcome Trust grants WT008150 and WT099141 (C.V.R.), and European Research Council IMPRESS grant ERC268851 (C.V.R.).

References

1. Zhao J, Benlekbir S, Rubinstein JL. Electron cryomicroscopy observation of rotational states in a eukaryotic V-ATPase. Nature. 2015; 521:241–245. [PubMed: 25971514]
2. Allegretti M, et al. Horizontal membrane-intrinsic α-helices in the stator a-subunit of an F-type ATP synthase. Nature. 2015; 521:237–240. [PubMed: 25707805]
3. Zhou A, et al. Structure and conformational states of the bovine mitochondrial ATP synthase by cryo-EM. eLife. 2015; 4:e10180. [PubMed: 26439008]
4. Morales-Rios E, Montgomery MG, Leslie AGW, Walker JE. Structure of ATP synthase from *Paracoccus denitrificans* determined by X-ray crystallography at 4.0 Å resolution. Proc Natl Acad Sci USA. 2015; 112:13231–13236. [PubMed: 26460036]
5. Schep DG, Zhao J, Rubinstein JL. Models for the a subunits of the *Thermus thermophilus* V/A-ATPase and *Saccharomyces cerevisiae* V-ATPase enzymes by cryo-EM and evolutionary covariance. Proc Natl Acad Sci USA. 2016; 113:3245–3250. [PubMed: 26951669]
6. Kane PM. Disassembly and reassembly of the yeast vacuolar H^+-ATPase *in vivo*. J Biol Chem. 1995; 270:17025–17032. [PubMed: 7622524]
7. Sumner JP, et al. Regulation of plasma membrane V-ATPase activity by dissociation of peripheral subunits. J Biol Chem. 1995; 270:5649–5653. [PubMed: 7890686]
8. Couoh-Cardel S, Milgrom E, Wilkens S. Affinity purification and structural features of the yeast vacuolar ATPase Vo membrane sector. J Biol Chem. 2015; 290:27959–27971. [PubMed: 26416888]
9. Benlekbir S, Bueler SA, Rubinstein JL. Structure of the vacuolar-type ATPase from *Saccharomyces cerevisiae* at 11-Å resolution. Nat Struct Mol Biol. 2012; 19:1356–1362. [PubMed: 23142977]
10. Qi J, Forgac M. Function and subunit interactions of the N-terminal domain of subunit a (Vph1p) of the yeast V-ATPase. J Biol Chem. 2008; 283:19274–19282. [PubMed: 18492665]
11. Powell B, Graham LA, Stevens TH. Molecular characterization of the yeast vacuolar H^+-ATPase proton pore. J Biol Chem. 2000; 275:23654–23660. [PubMed: 10825180]
12. Hirata R, Graham LA, Takatsuki A, Stevens TH, Anraku Y. *VMA11* and *VMA16* encode second and third proteolipid subunits of the *Saccharomyces cerevisiae* vacuolar membrane H^+-ATPase. J Biol Chem. 1997; 272:4795–4803. [PubMed: 9030535]
13. Nishi T, Kawasaki-Nishi S, Forgac M. The first putative transmembrane segment of subunit c" (Vma16p) of the yeast V-ATPase is not necessary for function. J Biol Chem. 2003; 278:5821–5827. [PubMed: 12482875]
14. Couoh-Cardel S, Hsueh Y-C, Wilkens S, Movileanu L. Yeast V-ATPase proteolipid ring acts as a large-conductance transmembrane protein pore. Sci Rep. 2016; 6
15. Matthies D, et al. High-resolution structure and mechanism of an F/V-hybrid rotor ring in a Na^+-coupled ATP synthase. Nat Commun. 2014; 5
16. Vik SB, Antonio BJ. A mechanism of proton translocation by F_1F_0 ATP synthases suggested by double mutants of the a subunit. J Biol Chem. 1994; 269:30364–30369. [PubMed: 7982950]
17. Junge W, Lill H, Engelbrecht S. ATP synthase: an electrochemical transducer with rotatory mechanics. Trends Biochem Sci. 1997; 22:420–423. [PubMed: 9397682]

18. Neale C, Chakrabarti N, Pomorski P, Pai EF, Pomès R. Hydrophobic gating of ion permeation in magnesium channel CorA. PLOS Comput Biol. 2015; 11:e1004303. [PubMed: 26181442]
19. Angevine CM, Herold KA, Fillingame RH. Aqueous access pathways in subunit a of rotary ATP synthase extend to both sides of the membrane. Proc Natl Acad Sci USA. 2003; 100:13179–13183. [PubMed: 14595019]
20. Toei M, Toei S, Forgac M. Definition of membrane topology and identification of residues important for transport in subunit a of the vacuolar ATPase. J Biol Chem. 2011; 286:35176–35186. [PubMed: 21832060]
21. Kühlbrandt W, Davies KM. Rotary ATPases: a new twist to an ancient machine. Trends Biochem Sci. 2016; 41:106–116. [PubMed: 26671611]
22. Pellegrini-Calace M, Maiwald T, Thornton JM. PoreWalker: a novel tool for the identification and characterization of channels in transmembrane proteins from their three-dimensional structure. PLOS Comput Biol. 2009; 5:e1000440. [PubMed: 19609355]
23. Smart OS, Neduvelil JG, Wang X, Wallace BA, Sansom MSP. HOLE: a program for the analysis of the pore dimensions of ion channel structural models. J Mol Graph. 1996; 14:354–360. [PubMed: 9195488]
24. Kawasaki-Nishi S, Nishi T, Forgac M. Arg-735 of the 100-kDa subunit a of the yeast V-ATPase is essential for proton translocation. Proc Natl Acad Sci USA. 2001; 98:12397–12402. [PubMed: 11592980]
25. Cain BD, Simoni RD. Impaired proton conductivity resulting from mutations in the a subunit of F_1F_0 ATPase in *Escherichia coli*. J Biol Chem. 1986; 261:10043–10050. [PubMed: 2874137]
26. DeCoursey TE. The voltage-gated proton channel: a riddle, wrapped in a mystery, inside an enigma. Biochemistry. 2015; 54:3250–3268. [PubMed: 25964989]
27. Bueler SA, Rubinstein JL. Vma9p need not be associated with the yeast V-ATPase for fully-coupled proton pumping activity *in vitro*. Biochemistry. 2015; 54:853–858. [PubMed: 25546637]
28. Nelson H, Nelson N. Disruption of genes encoding subunits of yeast vacuolar H^+-ATPase causes conditional lethality. Proc Natl Acad Sci USA. 1990; 87:3503–3507. [PubMed: 2139726]
29. Compton MA, Graham LA, Stevens TH. Vma9p (subunit e) is an integral membrane V_O subunit of the yeast V-ATPase. J Biol Chem. 2006; 281:15312–15319. [PubMed: 16569636]
30. MacCallum JL, Bennett WFD, Tieleman DP. Distribution of amino acids in a lipid bilayer from computer simulations. Biophys J. 2008; 94:3393–3404. [PubMed: 18212019]
31. Shevchenko A, Wilm M, Vorm O, Mann M. Mass spectrometric sequencing of proteins silver-stained polyacrylamide gels. Anal Chem. 1996; 68:850–858. [PubMed: 8779443]
32. Olsen JV, et al. Parts per million mass accuracy on an Orbitrap mass spectrometer via lock mass injection into a C-trap. Mol Cell Proteomics. 2005; 4:2010–2021. [PubMed: 16249172]
33. Marr CR, Benlekbir S, Rubinstein JL. Fabrication of carbon films with ~ 500nm holes for cryo-EM with a direct detector device. J Struct Biol. 2014; 185:42–47. [PubMed: 24269484]
34. Tivol WF, Briegel A, Jensen GJ. An improved cryogen for plunge freezing. Microsc Microanal. 2008; 14:375–379. [PubMed: 18793481]
35. Goddard TD, Huang CC, Ferrin TE. Visualizing density maps with UCSF Chimera. J Struct Biol. 2007; 157:281–287. [PubMed: 16963278]
36. Rubinstein JL, Brubaker MA. Alignment of cryo-EM movies of individual particles by optimization of image translations. J Struct Biol. 2015; 192:188–195. [PubMed: 26296328]
37. Mindell JA, Grigorieff N. Accurate determination of local defocus and specimen tilt in electron microscopy. J Struct Biol. 2003; 142:334–347. [PubMed: 12781660]
38. Zhao J, Brubaker MA, Benlekbir S, Rubinstein JL. Description and comparison of algorithms for correcting anisotropic magnification in cryo-EM images. J Struct Biol. 2015; 192:209–215. [PubMed: 26087140]
39. Scheres SHW. RELION: implementation of a Bayesian approach to cryo-EM structure determination. J Struct Biol. 2012; 180:519–530. [PubMed: 23000701]
40. Mastronarde DN. Automated electron microscope tomography using robust prediction of specimen movements. J Struct Biol. 2005; 152:36–51. [PubMed: 16182563]

41. Grant T, Grigorieff N. Automatic estimation and correction of anisotropic magnification distortion in electron microscopes. J Struct Biol. 2015; 192:204–208. [PubMed: 26278979]
42. Grant T, Grigorieff N. Measuring the optimal exposure for single particle cryo-EM using a 2.6 Å reconstruction of rotavirus VP6. eLife. 2015; 4:e06980. [PubMed: 26023829]
43. Rohou A, Grigorieff N. CTFFIND4: Fast and accurate defocus estimation from electron micrographs. J Struct Biol. 2015; 192:216–221. [PubMed: 26278980]
44. Grigorieff N. FREALIGN: high-resolution refinement of single particle structures. J Struct Biol. 2007; 157:117–125. [PubMed: 16828314]
45. Grigorieff N. Frealign: an exploratory tool for single-particle Cryo-EM. Methods Enzymol. 2016; 579:191–226. [PubMed: 27572728]
46. Penczek PA, et al. CTER-rapid estimation of CTF parameters with error assessment. Ultramicroscopy. 2014; 140:9–19. [PubMed: 24562077]
47. Cardone G, Heymann JB, Steven AC. One number does not fit all: mapping local variations in resolution in cryo-EM reconstructions. J Struct Biol. 2013; 184:226–236. [PubMed: 23954653]
48. Arnold K, Bordoli L, Kopp J, Schwede T. The SWISS-MODEL workspace: a web-based environment for protein structure homology modelling. Bioinformatics. 2006; 22:195–201. [PubMed: 16301204]
49. Emsley P, Cowtan K. Coot: model-building tools for molecular graphics. Acta Crystallogr D Biol Crystallogr. 2004; 60:2126–2132. [PubMed: 15572765]
50. Adams PD, et al. PHENIX: a comprehensive Python-based system for macromolecular structure solution. Acta Crystallogr D Biol Crystallogr. 2010; 66:213–221. [PubMed: 20124702]
51. Barad BA, et al. EMRinger: side chain-directed model and map validation for 3D cryo-electron microscopy. Nat Methods. 2015; 12:943–946. [PubMed: 26280328]

Europe PMC Funders Author Manuscripts

Europe PMC Funders Author Manuscripts

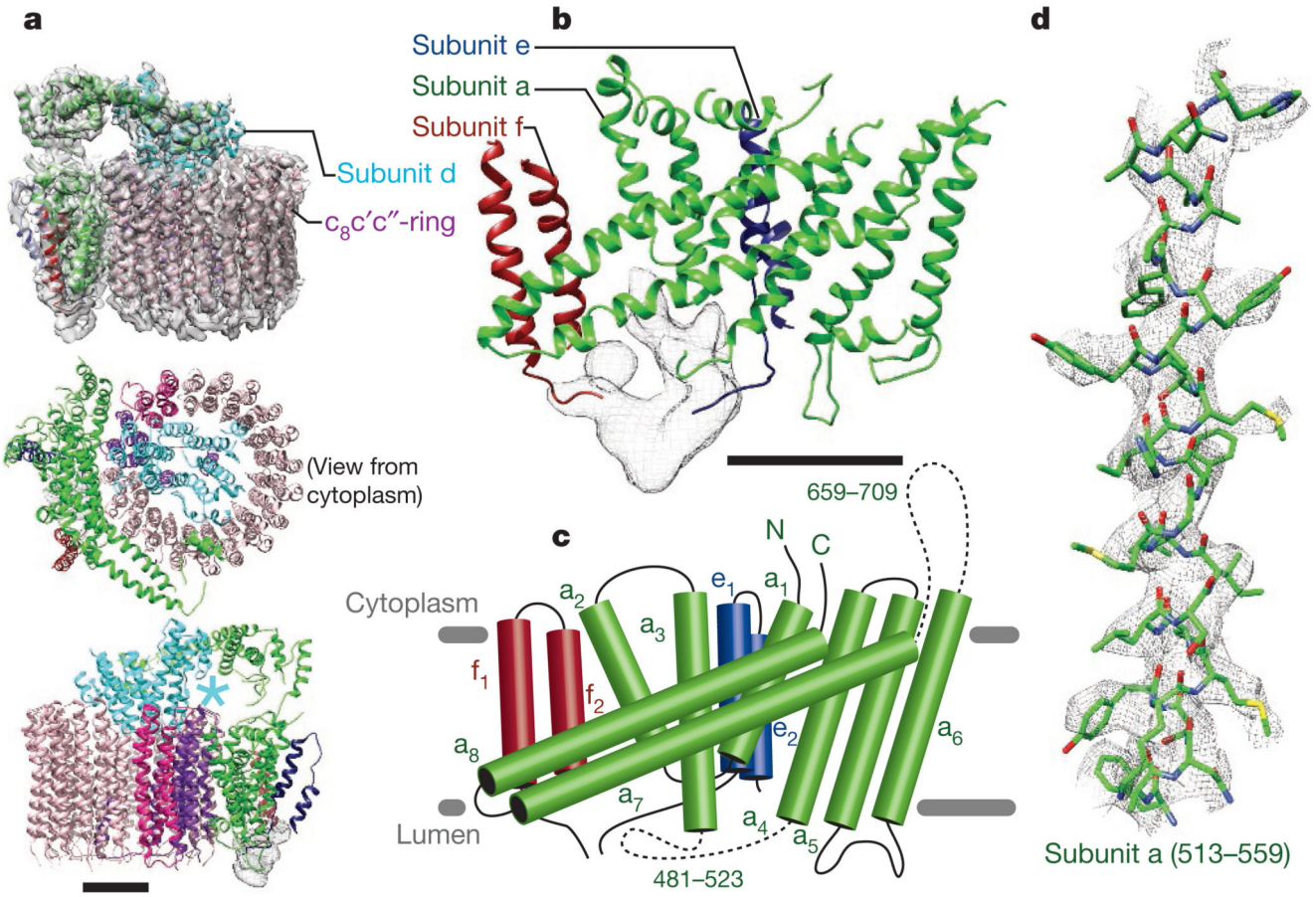

Figure 1. The intact V_O complex.

a, The V_O cryo-EM density map (semi-transparent surface, top) shows subunits a (green), c (pink), c′ (magenta), c″ (purple), d (cyan), e (blue), and f (red-brown). The asterisk indicates the contact between subunits d and c″. **b**, **c**, An enlarged view and cartoon of the C-terminal domain of subunit a with subunits e and f. Unfitted density is shown as grey mesh. **d**, An illustration of how the cryo-EM map allows atomic models to be built for most of the protein sequence. Scale bars, 25 Å.

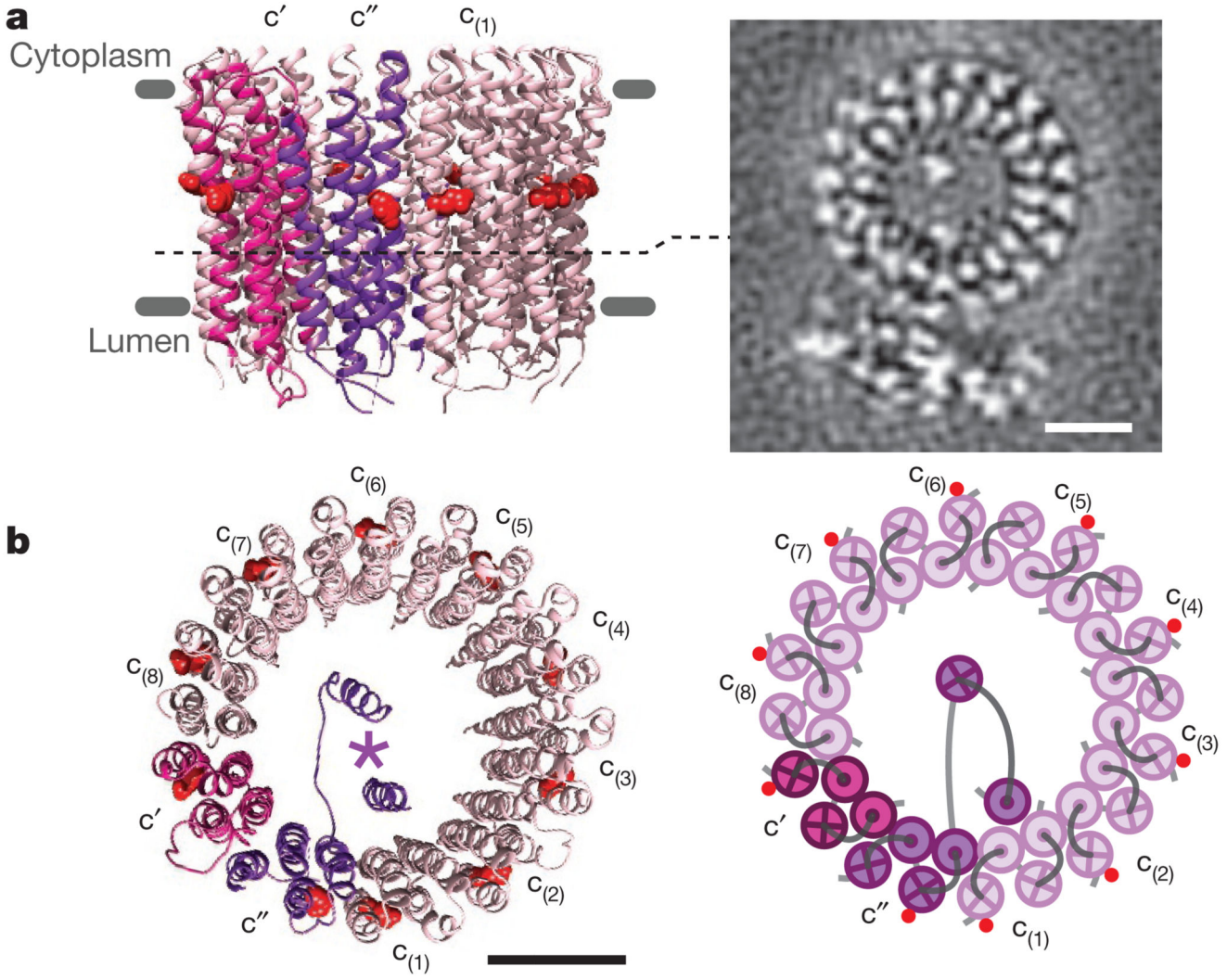

Figure 2. Asymmetry of the c-ring.

a, A ribbon model of the c-ring (left) with a map section (right) shows the two N-terminal α-helices of subunit c″ in the middle of the c-ring. **b**, A view of the c-ring model (left) and cartoon (right) from the cytoplasm shows the asymmetric distribution of mid-membrane Glu residues around the ring (red). The two N-terminal α-helices of subunit c″ are marked with an asterisk (left). Scale bars, 25 Å.

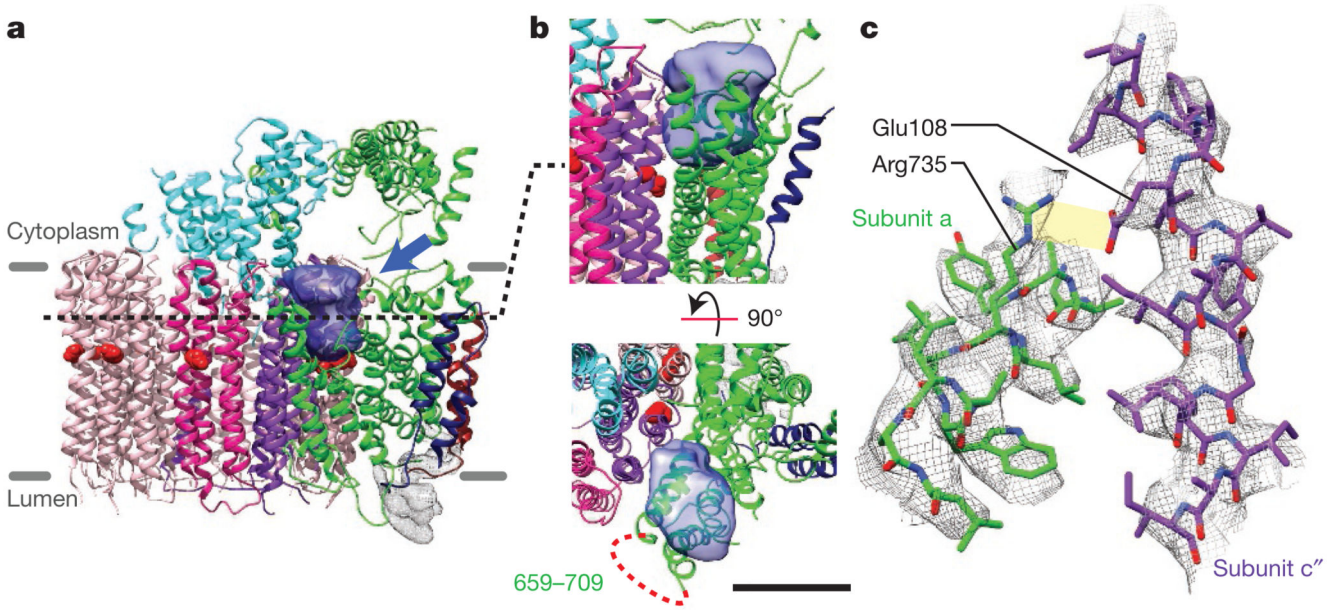

Figure 3. Cytoplasmic half-channel and subunit a/c-ring interaction.

a, **b**, A large cavity (blue density and arrow) is apparent between the c-ring and subunit a in the expected position of the cytoplasmic half-channel. The cavity is near the unresolved loop composed of residues 659 to 709 from subunit a (bottom of **b**, dashed red line). Scale bar, 25 Å. **c**, At the mid-membrane terminus of the cavity, the essential residues Arg735 from subunit a and Glu108 from subunit c″ are positioned to interact.

Europe PMC Funders Author Manuscripts

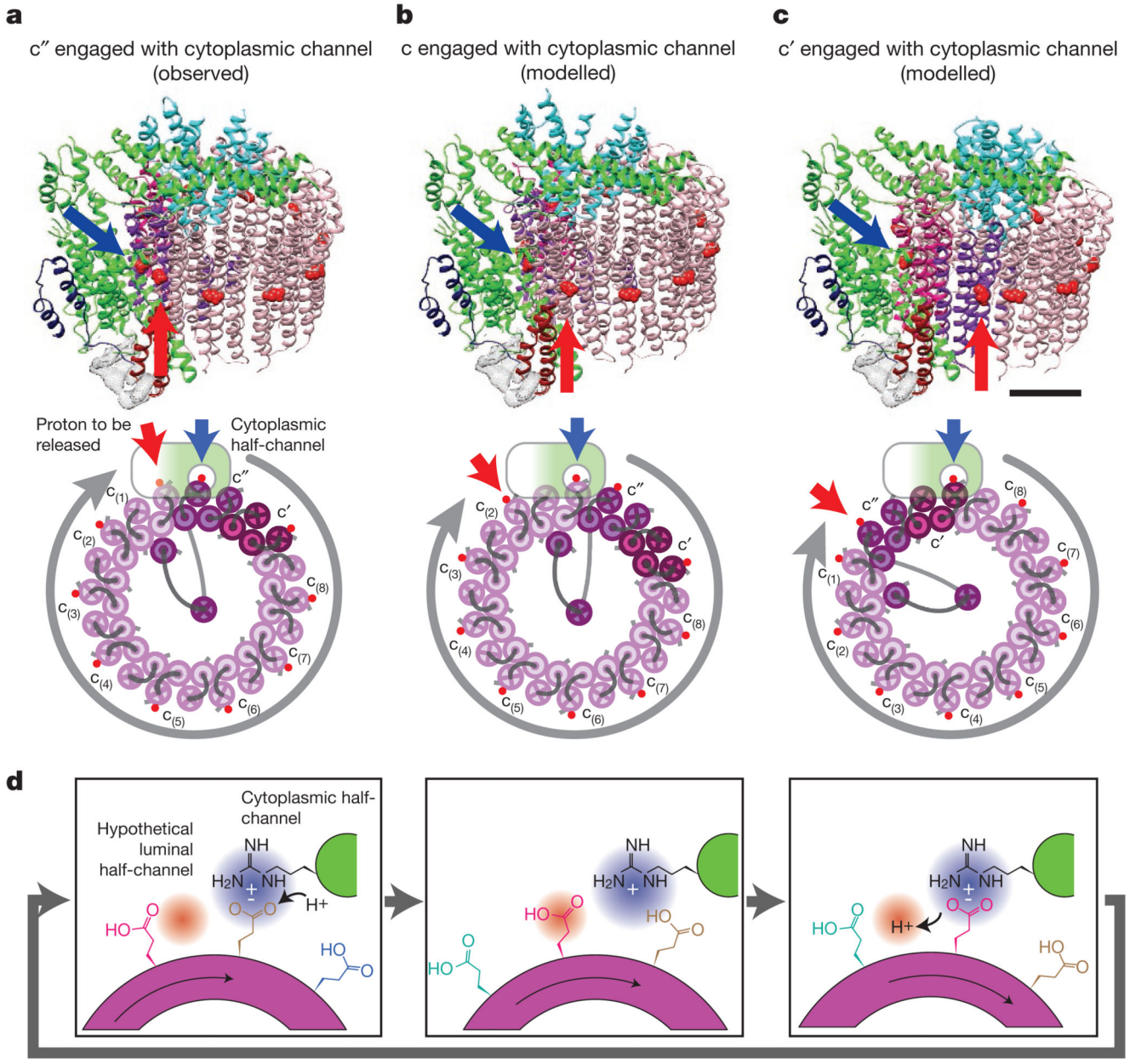

Figure 4. Irregularly spaced Glu residues require protonation before deprotonation.

a, The observed structure (top) with cartoon (bottom) illustrates that when Glu108 of subunit c″ is aligned with the cytoplasmic half-channel (blue arrow), Glu137 of subunit $c_{(1)}$ contacts subunit a (red arrow) and could be aligned with a luminal half-channel. **b**, When Glu137 of a subunit c is aligned with the cytoplasmic half-channel (blue arrow) Glu137 of the next subunit c is not in contact with subunit a (red arrow). **c**, When Glu145 of subunit c′ is aligned to the cytoplasmic half-channel (blue arrow) Glu108 of subunit c″ is too far from subunit a to interact (red arrow). Scale bar, 25 Å. **d**, The sequence of protonation and

deprotonation events that occur during c-ring rotation, with each Glu residue given its own colour.

Europe PMC Funders Author Manuscripts